Aerosol features retrieved from solar aureole data: a simulation study concerning a turbid atmosphere

G. Tonna, T. Nakajima, and R. Rao

The characteristics of the solar aureole were evaluated for several cases of a turbid atmosphere in the 3° $\leq \Theta \leq$ 30° interval of scattering angles; for each case, the features of the aerosol were retrieved from the simulated aureole data. Computations were carried out with a recently set up radiative transfer code that uses the approximated delta-M method, corrected further for the 1st and 2nd scattering orders. Results showed that the software tested can work out both the direct and the inverse aureole problems with great accuracy and efficiency in several different situations, so it can reliably be used for handling experimental data measured in the field with an aureolemeter. Furthermore, the input parameters of ground albedo, complex refractive index, aerosol radius interval, and measurement angles were varied within a set of values to examine the sensitivity of the retrieval to improperly assumed values of these parameters and to evaluate the most suitable way of determining their correct values. Only data concerning diffuse radiation were elaborated. Results showed that (1) the scanned scattering angles have to be extended up to 40°; (2) the most suitable radius interval for aerosols appears to be from 0.05 to 15 μm; (3) ground albedo A should be independently determined within 15%; and (4) as to the complex refractive index $\tilde{m}$, the real part should be given within 3.5%, and the imaginary part within from 10% to 50%, according to its value. Finally, a procedure through which it is possible to derive A and $\tilde{m}$ by extending the information content of the aureole data is discussed. Improved calibration procedures are also proposed.

Key words: Solar aureole, multiple scattering.

1. Introduction

Knowledge of the parameters that determine the optical properties of the atmospheric aerosol (size distribution and refractive index) is essential for the determination of the effect of atmospheric aerosol on the climate and for the control of the air quality. The determination of these parameters can be greatly facilitated by the use of the aureole technique, which from measurements of direct and diffuse solar radiation allows one to derive the aerosol extinction and the single-scattering phase function, from which the aerosol parameters are finally determined.

The solar aureole is the region of enhanced brightness that surrounds the solar disk in cloudless conditions and is mainly due to the forward single-scattering of light by the aerosol particles; the solar light through successive scattering processes propagates within the whole atmosphere, giving rise to the diffuse radiation E, and the unscattered light constitutes the direct radiation F. The device used for measuring the sky radiation is the sky radiometer, or aureolemeter, which is constituted by a photometer with annexed interferential filters for the selection of the wavelengths at which to operate and a pointing system; when the aureolemeter points toward the Sun it measures the direct radiation, actually working as a Sun photometer. The wavelengths are usually selected within the main atmospheric windows in the visible and the near infrared to reduce the radiative transfer problem to a pure scattering problem; the aureolemeter used in our research program (Model Pom-01, produced by Finetec) uses the following wavelengths: 0.369, 0.500, 0.675, 0.776, 0.862 and 1.048 μm.

Measurements are usually carried out with the aureolemeter pointed along a conical surface with the same zenith angle of the Sun (almucantar) or along a plane with the same azimuth angle of the Sun (principal plane); details on this geometry are given in Appendix A. The connection between the aerosol phase function and the solar sky intensity occurs

G. Tonna and R. Rao are with the Institute for Atmospheric Physics, Consiglio Nazionale delle Ricerche, Rome, Italy. T. Nakajima is with the Center for Climate System Research, University of Tokyo, 4-6-1 Komaba, Meguro-ku, Tokyo, Japan.

Received 7 March 1994; revised manuscript received 25 January 1995.

0003-6935/95/214486-14$06.00/0.

through the radiative transfer equation (RTE) in the multiple-scattering scheme. The benefits that arise from adding measurements of diffuse radiation to measurements of extinction are the following: the calibration of the aureolemeter when it is measuring E depends only on its field of view; the calibration of direct readings can be improved by the use of diffuse radiation data; the detectable radius range of the aerosol particles is from approximately 0.05 to 10 μm; as the intensity E is proportional to the total optical thickness τ, the inversion procedure is very stable even for small τ.

The characteristics of the solar aureole were studied by several authors. Box and Deepak[1] used the Gauss–Seidel iterative scheme to compute single- and multiple-scattering contributions to the aureole in the solar almucantar and in the principal plane, at the wavelength $\lambda = 0.55$ μm, for a plane-parallel atmosphere composed of air molecules, ozone, and aerosol particles. Results showed that in the near-forward direction the multiple-scattering contribution is significant for optical depths of 0.4, and the shape of the angular distribution of almucantar intensity up to 10° appeared only slightly sensitive to multiple scattering.

Arao and Tanaka[2] computed spectral and angular distributions of the intensity of the solar aureole for realistic models of the turbid atmosphere by means of a matrix-doubling method applied to a homogeneous plane-parallel atmosphere. Results showed that the effect of aerosol multiple scattering cannot be ignored, as the single-scattering theory breaks down for almost all wavelengths and turbidity conditions; the contributions of light reflected from the ground surface were also shown to be significant.

Arao and Tanaka[3] considered the effect of additional circumsolar radiation on the measurement of direct solar radiation and on the determination of the turbidity parameters.

The formulation of the aureole inverse problem developed over the years from the first single-scattering formulations[4] to the recent accurate and efficient code based on the improved multiple and single scattering components (IMS) method and used in this paper.

Deepak[4] worked out the single-scattering approximation for the intensity in the almucantar and studied the conditions that make the inversion problem tractable.

Box and Deepak[5] computed almucantar intensities at $\lambda = 0.4$, 0.5, and 0.6 μm, with a multiple-scattering approximation to the RTE based on the Deirmendjian[6] perturbation method, which includes contributions that are due to single scattering by aerosol and molecules and to multiple scattering by molecules alone, while ignoring multiple-scattering events in which aerosols are involved; the approximation used has the advantage of retaining the formal structure of the single-scattering formulation.

Weinman *et al.*[7] used an analytical solution to the RTE in the small-angle approximation; the aerosol phase function and the Rayleigh molecular phase function were approximated by the sum of several Gaussian functions. The sunlight intensity was then inverted to yield the aerosol phase function at small angles with a nonlinear least-squares algorithm. In a connected paper Twitty[8] showed how to derive aerosol size distributions from the phase function by the use of a nonlinear iterative method.

Nakajima *et al.*[9] improved the approximation of Weinman *et al.*[7] by completing the spike of the aerosol phase function with an expansion of its residue in Legendre polynomials. The procedure for solving the RTE makes use of the analytical solution by Weinman *et al.*[7] and of a matrix-operator method developed by Tanaka and Nakajima.[10] The aerosol phase function was obtained from actual aureole data with an iterative algorithm, and the aerosol volume size distribution was obtained from both aureole and extinction data through a linear inversion.

Nakajima and Tanaka[11] developed a very reliable and efficient algorithm (the IMS method) to compute direct and diffuse solar radiation that uses a matrix formulation of the discrete-ordinate theory together with the delta-M approximation[12] to the aerosol phase function; the solution is further corrected for the 1st and 2nd scattering orders. With this procedure the calculated intensity follows the exact values with an accuracy of better than 1% for all the emergent directions, with a small number of quadrature points for integrating the RTE. This method constitutes the basis for the AUR.pack code used in this paper.

Several measurements of sky radiation and retrievals of aerosol features were carried out; ground-based measurements can be found in Refs. 13–18, and airborne measurements are found in Refs. 19–22.

In this paper we present simulated aureole data and related aerosol retrieval in several situations concerning a turbid atmosphere, with the aim of testing the reliability of the retrieval program to be used for treating actual data. Below we carry out a study on the consequences of an uncertain evaluation of several input parameters on the retrieval procedure and consider the problem connected with their determination. Mainly data concerning diffuse radiation were elaborated, as their treatment constitutes the crucial point for the practical use of the aureole technique.

2. Theory and Computations

The quantities that can be measured in a cloudless sky by the use of the solar radiation as a source are the direct radiation flux F and the diffuse intensity E as a function of wavelength. The direct flux F [in watts times inverse square meters per micrometer (W m^{-2} μm^{-1})] is expressed as

$$F = F_0 \exp(-m\tau), \tag{1}$$

where F_0 is the flux at the upper limit of the atmosphere, τ is the total optical thickness, θ_0 the Sun zenith angle, and $m = 1/\cos\theta_0$ is the optical air mass. The intensity E (W m^{-2} μm^{-1}) is determined through

the RTE and in the almucantar geometry is expressed as

$$E(\theta_0, \phi) \equiv E(\Theta) = m\omega\tau P(\Theta)F\Delta\Omega + q(\Theta), \qquad (2)$$

where ϕ is the observation azimuth angle, Θ is the scattering angle, ω is the single-scattering albedo of the whole air mass, $P(\Theta)$ is the total phase function, $\Delta\Omega$ is the solid view angle of the aureolemeter,[20] and $q(\Theta)$ indicates the multiple-scattering contribution. We now consider the intensity normalized by the direct radiation flux, that is, the ratio

$$R(\Theta) \equiv \frac{E(\Theta)}{Fm\Delta\Omega} = \omega\tau P(\Theta) + r(\Theta), \qquad (3)$$

with $r(\Theta)$ as the MS contribution, which is a more stable and accurate quantity than E and is used here with F for deriving the aerosol properties. Similar considerations hold for E and R in the principal plane. From simulated or measured F and R data, the features of the aerosol can be retrieved; note that before τ and R actually become available for inversion, one needs to perform two calibrations, which amounts to determining F_0 and $\Delta\Omega$ at each wavelength considered.

Simulated R and τ data, and related inversions, were worked out with the software package AUR. pack, supplied by Nakajima and based on the IMS method[11,20] for handling the RTE, together with linear and nonlinear inversion methods; this software allows one to produce accurate data on direct and diffuse sky radiation and to run the inversion procedure efficiently, providing results within 60 s. The retrieval of simulated or measured data proceeds by the use of iteration; the size distribution is recovered in the shape of a histogram, with 20 size intervals. Mie intensity functions and efficiency factors for spherical particles were computed in advance at 55 grid points for Θ [0(0.2)1(0.5)5(1)10(2.5)20(5)180°] and at 59 grid points for the size parameter (logarithmically spaced from 5.42×10^{-2} to 5.84×10^{2}); as a consequence, measurement angles are determined from Eqs. (A2)–(A5) by first selecting the values of Θ at which we want to reconstruct the aerosol phase function $P_A(\Theta)$. The maximum number of loops and the tolerance parameter for convergence were set as 20 and 0.001, respectively.

Four different modes of operation are available in the retrieval program, as selected by the index INDM, to face different possible experimental conditions:

(1) INDM = 2. The optical thicknesses of aerosol, τ_A, are not known, which can be because, for instance, the Sun photometer has not been calibrated. In this case[20] the inversion relies entirely on $R(\Theta)$, which is inverted to determine the aerosol volume radius distribution $v(r)$ as well as τ_A. The algorithm that is adopted starts from initial values of $P_A(\Theta)$ and $\tau_A(\lambda)$, computes $R^n(\Theta)$ at the nth step through the IMS radiative scheme, and obtains $P_A{}^{n+1}(\Theta)$ by comparing $R^n(\Theta)$ with the corresponding experimental data; from $P_A{}^{n+1}(\Theta)$ the algorithm obtains a new approximation for $v(r)$, and from this a new approximation for $\tau_A(\lambda)$ is obtained, and then the algorithm iterates the procedure.

(2) INDM = 0. The τ_A are determined with an improved procedure (see Section 4) for determining F_0, which allows one to determine F_0 within 1% and, as a consequence, τ_A within 5%, the accuracy depending on λ and on the product $m\tau$. In this case the τ_A are kept fixed and used with $R(\Theta)$ in the retrieval. From F one derives τ, and the forward lobe of the phase function is derived from intensity measurements by means of an iterative algorithm; the function $v(r)$ is subsequently determined through the simultaneous inversion of data of $\tau_A(\lambda)$ and $P_A(\Theta)$, by means of a constrained linear method.[9]

(3) INDM = 1. Only indicative values of τ_A are known, as occurs with the normal Langley plot, which usually determines F_0 within 10% and, as a consequence, τ_A within 50%. In this case the τ_A are used in the inversion, together with the $R(\Theta)$ data, only as first-guess values, and are updated at each step. The τ_A data can be given different weights, according to their reliability.

(4) INDM = −1. The view angle of the aureolemeter is not known, so that the inversion depends on the τ_A, which are used to normalize the $R(\Theta)$ data.

Starting from several models of atmosphere defined by the Sun zenith angle, scanning geometry (almucantar or principal plane, as well as number and values of the selected measurement angles), ground albedo, aerosol volume spectrum, and complex refractive index, simulated aureole data and optical thicknesses were computed at selected wavelengths; these data were then inverted to recover the aerosol volume spectrum. The wavelengths selected were 0.369, 0.500, 0.675, 0.776, 0.862, and 1.048 μm; one index of refraction $\tilde{m} = m - ki$ was assumed for all the six wavelengths, because of its small variations with λ for the spectral interval considered. Before the retrieval procedure starts, the following parameters have to be defined: ground albedo A, complex refractive index, radius interval for the aerosol particles, maximum number of loops in the iteration procedure, number of size intervals to be considered, and tolerance parameter for convergence.

The aerosol model spectra used for the present study are the following:

Model 1. Urban model by Shettle and Fenn.[23] This is a bimodal spectrum concerning urban aerosol and given by the sum of two log normals as

$$v(r) \equiv \frac{dV}{d\ln r} = C_1 \exp\left\{-\frac{1}{2}\left[\frac{\ln(r/r_1)}{\ln s_1}\right]^2\right\} + C_2 \exp\left\{-\frac{1}{2}\left[\frac{\ln(r/r_2)}{\ln s_2}\right]^2\right\}. \qquad (4)$$

Here $dV/d\ln r$ is the columnar volume size distribution with logarithmic radius interval [in cubic centime-

ters per square centimeter (cm^3/cm^2)]. The urban model was taken to be a mixture of water-soluble substances (ammonium and calcium sulfate, plus organic compounds), dustlike aerosols, and carbonaceous particles. The parameters for this model at a relative humidity of 70% are the following: $C_1 = 2.29$, $r_1 = 0.20$, $s_1 = 2.24$, $C_2 = 3.10$, $r_2 = 6.09$, $s_2 = 2.51$. Minimum and maximum radii were assumed as $r_m = 0.05$ μm and $r_M = 20$ μm; the refractive index is $\tilde{m} = 1.48 - 0.055i$. As the parameters r_m and r_M are not given in the original report,[23] they were selected by us on the basis of the behavior of the size distribution.

Model 2. This bimodal spectrum concerns tropospheric aerosol and was retrieved by Shiobara *et al.*[18] from measurements of the solar aureole taken in the suburbs of Sendai, Japan. It is given by the sum of two log normals with the following parameters: $C_1 = 2.65$, $r_1 = 0.21$, $s_1 = 1.97$, $C_2 = 1.28$, $r_2 = 2.98$, $s_2 = 2.17$; $r_m = 0.1$ μm, $r_M = 10$ μm. The refractive index was taken as $\tilde{m} = 1.50 - 0.01i$.

As we describe the atmosphere with only one layer in both the direct and the inverse problems, the spectra have to be understood as representative of the whole layer. Besides, in computing simulated data, the two constants C_1 and C_2 are adjusted by the program so as to correctly reproduce the input datum τ_A (0.5 μm).

3. Retrieval of Simulated Aureole Data

We consider nine cases of retrieval from simulated data; the retrievals were carried out for all four available modes (index INDM). The results of the inversions are summarized in Table 1.

A. Model 1, Cases 1–4

Four cases of simulations that concern the urban model by Shettle and Fenn,[23] Model 1, are presented:

Case 1. The following input data have been used: $\theta_0 = 30°$, $A = 0.25$, τ_A (0.5 μm) = 0.2, almucantar geometry. The aureole data are shown in Fig. 1, in which the aerosol optical thicknesses at the six wavelengths considered are also given; the aureole data are in agreement with similar data by other authors.[2,5] In Fig. 1 we have $6° \leq \phi \leq 62.4°$; this is due to the fact that in setting up the input data for simulations we chose to determine $R(\Theta)$ in the range $3° \leq \Theta \leq 30°$, which according to Eq. (A2) implies $6° \leq \phi \leq 62.4°$. Results concerning retrieved data are shown in Fig. 2 and in Table 1. In the middle part of Fig. 2 the relative difference between the retrieved (v^r) and the given (v^g) size distributions, defined as $\epsilon(\%) = (v^r - v^g)/v^g$, is reported as a function of r; in the lower part of Fig. 2 $C_{\max}$ is the maximum contribution of each portion v_j of the inverted volume spectrum to any of the data used in the retrieval (R for INDM = 2 and 1, R and τ_A for INDM = 0 and −1). From Fig. 2 we show that $\epsilon(\%)$ increases toward the right- and the left-hand sides of the considered radius interval (0.05–20 μm), reaching values of around 60% at the limits of the interval; this behavior is linked to the information content of the optical data, which is mainly connected with the central part of the considered radius interval and expressed by the parameter $C_{\max}$. As, according to previous results,[24] those portions of the interval for which $C_{\max} \geq 10\%$ are in close agreement with the true spectrum, by averaging $\epsilon(\%)$ over them the global rms relative deviation $\epsilon(v)$ given in the tables was computed. Besides $\epsilon(v)$, in the tables the rms relative deviations $\epsilon(R)$ between the simulated aureole data and those reconstructed through the retrieved volume size distribution, averaged on the scattering angles, are reported. Furthermore, the deviations concerning the aerosol optical thicknesses and defined as $\epsilon(\tau_A) = (\tau_A{}^r - \tau_A{}^g)/\tau_A{}^g$, are also reported; the deviations $\epsilon(P_A)$ were not reported because we always found that $\epsilon(P_A) \cong \epsilon(R)$, in agree-

Table 1. Case 1 (Aerosol Urban Model by Shettle and Fenn[23]) and Case 5 (Aerosol Tropospheric Model by Shiobara *et al.*[18]): Mean Relative Deviations (in Percent) between Simulated and Retrieved Data, Concerning Aureole Data, Aerosol Optical Thickness, and Volume Size Distribution[a]

	INDM = 2			INDM = 0			INDM = 1			INDM = −1		
λ (μm)	R	τ_A	v	R	τ_A	v	R	τ_A	v	R	τ_A	v
Case 1												
0.369	0.0	1.7		0.1	0.0		0.0	0.0		0.1	0.0	
0.500	0.0	1.0	1.67	0.1	0.0	0.64	0.0	0.0	0.68	0.1	0.0	0.67
0.675	0.0	0.8		0.1	0.1		0.0	0.1		0.1	0.1	
0.776	0.0	0.8		0.0	0.1		0.0	0.1		0.1	0.1	
0.862	0.1	0.9		0.1	0.1		0.1	0.1		0.1	0.1	
1.048	0.0	0.9		0.1	0.1		0.0	0.1		0.1	0.1	
Case 5												
0.369	0.1	0.2		0.1	0.1		0.1	0.2		0.1	0.2	
0.500	0.1	−0.2	1.47	0.2	−0.2	1.00	0.1	−0.2	0.87	0.1	−0.2	0.59
0.675	0.0	−0.1		0.1	−0.1		0.0	−0.1		0.0	−0.1	
0.776	0.1	0.0		0.0	0.0		0.1	0.0		0.1	0.1	
0.862	0.2	0.0		0.1	0.0		0.1	0.0		0.1	0.0	
1.048	0.1	0.0		0.1	0.0		0.1	0.0		0.0	0.0	

[a] $\epsilon(v)$ is included for $\lambda = 0.500$ μm for convenience, as it is independent of wavelength.

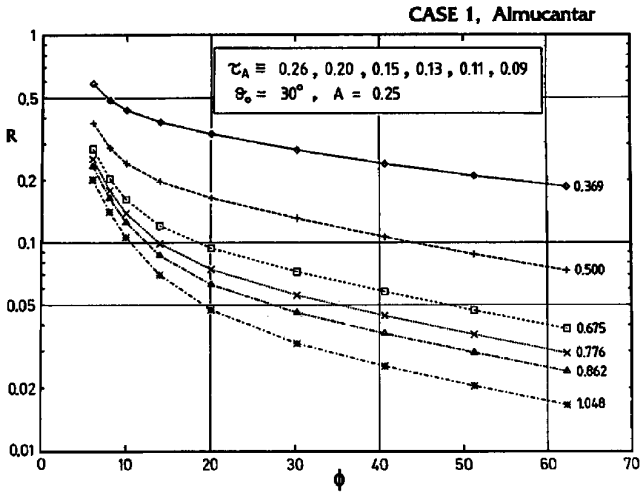

Fig. 1. Behavior of the ratio R with the azimuth angle ϕ, in the almucantar geometry, for case 1 and the conditions given in the labels. Wavelengths (in micrometers) are specified on the right-hand side of each curve.

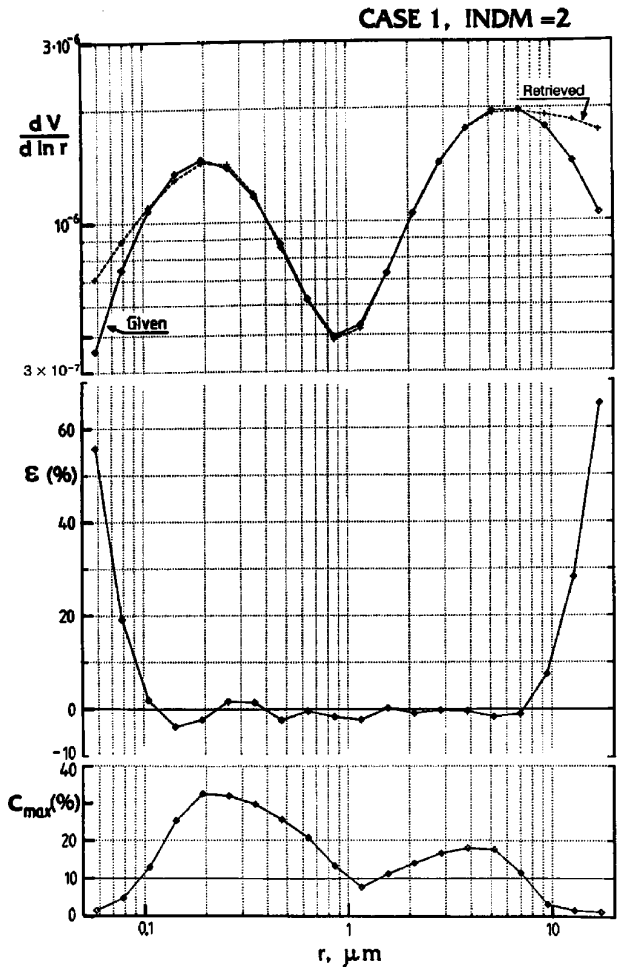

Fig. 2. Case 1: Top curve, given and retrieved size distributions; middle curve, relative difference between the given and retrieved size distributions, as a function of r, in percent; bottom curve, maximum contribution of each size interval to the phase function, in percent.

ment with Eq. (3), which shows an approximate linear relation between R and P. Table 1 shows that $\epsilon(R)$ and $\epsilon(\tau_A)$ are generally within 0.3%, and $\epsilon(v)$ is within 1%, showing no particular behavior as a function of the wavelength and the mode used in the retrieval. The only exception concerns the mode INDM = 2, which furnishes optical thicknesses of aerosol slightly worse than the other modes, in agreement with the fact that it uses only data of diffuse intensity.

Case 2. Input data are $\theta_0 = 60°$, $A = 0.25$, τ_A (0.5 μm) = 0.3, and almucantar geometry. In this case $3.5° \le \phi \le 34.8°$, as we chose $3° \le \Theta \le 30°$.

Case 3. Input data are $\theta_0 = 45°$, $A = 0.1$, τ_A (0.5 μm) = 0.4, and almucantar geometry. In this case $4.2° \le \phi \le 42.9°$.

Case 4. Input data are $\theta_0 = 20°$, $A = 0.2$, τ_A (0.5 μm) = 0.3, and principal-plane geometry; the data were computed starting from near the Sun position ($\theta = 17°$, $\phi = 0°$), going toward the zenith and then continuing in the same direction ($\phi = 180°$) up to $\theta = 10°$; according to Eqs. (A3)–(A5) $3° \le \Theta \le 30°$.

Results concerning cases 2–4 are almost exactly the same as those for case 1 given in Table 1, so they were not reported.

B. Model 2, Cases 5–9

Five cases of simulations that concern the tropospheric aerosol model by Shiobara *et al.*,[18] Model 2, are presented here.

Case 5. The following input data have been used: $\theta_0 = 30°$, τ_A (0.5 μm) = 0.2, $A = 0.25$, and almucantar geometry. In this case $6° \le \phi \le 62.4°$, $3° \le \Theta \le 30°$. From the results given in Table 1 one can see that the relative deviations $\epsilon(R)$ and $\epsilon(\tau_A)$ are within 0.2%, and $\epsilon(v)$ is within 1.5%, and no particular behavior as a function of the wavelength and the mode used in the retrieval is shown.

Case 6. Input data are $\theta_0 = 30°$, τ_A (0.5 μm) = 0.4, $A = 0.25$, and almucantar geometry.

Case 7. Input data are $\theta_0 = 30°$, τ_A (0.5 μm) = 0.4, $A = 0.1$, and almucantar geometry.

Case 8. Input data are $\theta_0 = 60°$, τ_A (0.5 μm) = 0.3, $A = 0.2$, and almucantar geometry. In this case $3.5° \le \phi \le 35°$, $3° \le \Theta \le 30°$.

Case 9. Input data are $\theta_0 = 30°$, τ_A (0.5 μm) = 0.2, $A = 0.25$, and principal-plane geometry. In this case data were computed starting from near the Sun position ($\theta = 27°$, $\phi = 0°$) and going toward the zenith ($\theta = 0°$); according to Eqs. (A3)–(A5) we have $3° \le \Theta \le 30°$.

Results concerning cases 6–9 are almost exactly the same as those given for case 5 in Table 1, so they were not reported.

From the data shown in this section one can see that the code used can work out the inverse aureole problem with great accuracy and efficiency. As to the direct problem, data such as those shown in Fig. 1 are in agreement with previous computations and

measurements found in the literature[2,5]; besides, an accurate test by Nakajima and Tanaka,[11] which was carried out in several conditions concerning both homogeneous and inhomogeneous atmospheres, showed that aureole data obtained with the present code are within 1% of true values obtained with the discrete-ordinate method. As a consequence, we can conclude that the code used is very suitable for handling the whole aureole problem.

On the other hand, the results shown in Table 1 turned out to be very good as, for instance, the inversion for INDM = 1 was carried out with the true values of τ_A, and for INDM = −1 with $\Delta\Omega$ included in the simulated R data; further simulations showed that, starting with τ_A values affected by a 20% error, INDM = 1 gives us retrieved values within 2% of the true values. Furthermore, before starting the inversion procedure, we simply assigned for the input parameters their true values, that is, the same values used in simulating the measurement data. With reference to the cases considered in this section, we examine in Section 4 the problems that occur in the actual selection of five such parameters and the consequences for the retrieval procedure of their possible wrong evaluation.

4. Sensitivity to the Input Parameters

The parameters considered are the following: measurement angles, retrieved aerosol radius interval, ground albedo, and real and imaginary parts of the complex refractive index. Data were elaborated for the INDM = 2 mode only, as it is the most important mode within the whole strategy of inversion for the practical use of the aureole technique. Indeed, the values of τ_A coming from data concerning only diffuse radiation constitute the starting point for the calibration of the aureolemeter when one is measuring the direct radiation, whereas data on τ_A and v coming from this mode can be the only available data when direct radiation cannot be reliably measured or handled.

In elaborating the data in Table 1, we used data on $R(\Theta)$ in the range $3° \le \Theta \le 30°$, even if greater angles were usually available according to the geometric situation selected. The lower limit of $\Theta = 3°$ is connected to the geometry of the aureolemeter, and the upper limit of $\Theta = 30°$ was assumed because it is generally agreed that the information content concerning the aerosol size distribution and the connected quantities R, P_A, τ_A is mainly included within the forward lobe of the phase function. This can be seen, at least approximately, from the behavior of the kernel functions for scattering and extinction entering the expressions of the aerosol phase function and optical thickness, which are respectively defined as

$$K(x) = (3/8\pi)\,\frac{[i_1(\Theta, x, \tilde{m}) + i_2(\Theta, x, \tilde{m})]}{x^3},$$

$$K_e(x) = \left(\frac{3}{4x}\right) Q_e(x, \tilde{m}), \tag{5}$$

where $x = 2\pi r/\lambda$ is the size parameter; i_1 and i_2 are the Mie intensity functions, and Q_e is the extinction coefficient; these functions, normalized to their integral over x, are reported in Fig. 3 for Model 2 ($\tilde{m} = 1.5 - 0.01i$). One can see that in the interval $3° \le \Theta \le 30°$ the kernel functions for scattering have reliable information content approximately within the interval $1 \le x \le 60$, which means that $0.05 \le r \le 10$ μm for our wavelength set, so that the chosen angular interval is sufficient for deriving $v(r)$ and reliably reconstructing the connected quantities R, P_A, τ_A, as shown by the results of Table 1. For Model 1 ($\tilde{m} = 1.48 - 0.055i$) the above size interval for scattering comes out to be exactly the same. We examined the effect of changing the upper value of Θ, Θ_U by taking into account that according to Eqs. (A1)–(A5) $\Theta_{max} = 2\theta_0$ for the almucantar geometry and $\Theta_{max} = 90° + \theta_0$ for the principal-plane geometry. Table 2 shows results concerning cases 1 to 4 when Θ_U is changed; from these data we show that better results can be obtained if Θ_U is slightly greater than 30° ($\Theta_U = 40°$ appears to be a good compromise). We note that among the quantities considered, that is, R, τ_A, and v, only R can be controlled in an actual situation through $\epsilon(R)$. On the other hand, as according to the results of Table 2 $\epsilon(R)$ practically does not vary with Θ_U, we were forced to try locating an *a priori* optimal value for Θ_U.

When elaborating the data of Table 1, we assumed the same radius interval both in computing and in inverting the aureole data. On the other hand, when retrieving actual field data, we do not know the radius interval concerning the aerosol particles in advance, and we need to fix it in the retrieval program; besides, we may possibly need to fix a unique

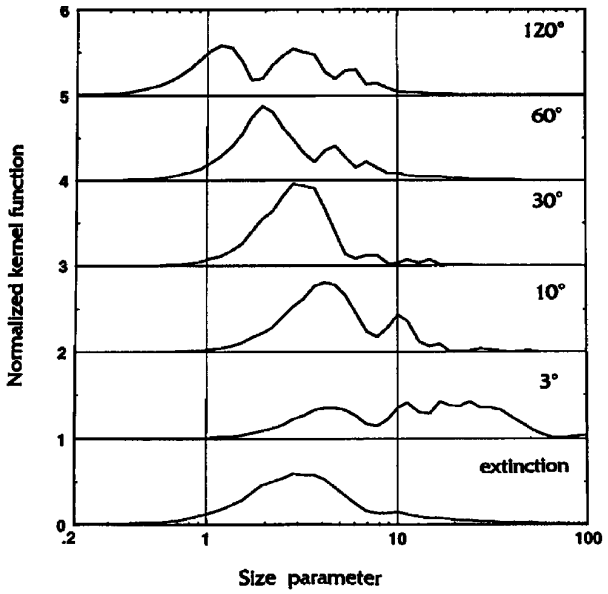

Fig. 3. Behavior of the normalized kernel functions for extinction and for scattering at five angles as a function of the size parameter $x = 2\pi r/\lambda$. The complex refractive index was assumed to be $\tilde{m} = 1.5 - 0.01i$ (aerosol Model 2). The kernel functions are normalized to 1 and shifted upward.

Table 2. Mean Relative Deviations (in Percent) between Simulated and Retrieved Data for Cases 1–4 and Different Selections of the Upper Value of Θ (in Degrees)[a]

	20°			30°			40°			50°			60°			70°			90°			120°		
λ (μm)	R	τ_A	v	R	τ_A	v	R	τ_A	v	R	τ_A	v	R	τ_A	v	R	τ_A	v	R	τ_A	v	R	τ_A	v
Case 1																								
0.369	0.1	3.6		0.0	1.7		0.1	1.7		0.8	−3.7		0.1	0.5										
0.500	0.0	2.0	2.04	0.0	1.0	1.67	0.1	1.0	1.60	0.3	−1.9	4.41	0.1	0.4	2.15									
0.675	0.0	1.5		0.0	0.8		0.1	0.8		0.3	−1.2		0.1	0.4										
0.776	0.0	1.4		0.0	0.8		0.0	0.8		0.3	−1.1		0.0	0.5										
0.862	0.1	1.4		0.1	0.9		0.1	0.9		0.1	−1.0		0.1	0.5										
1.048	0.0	1.5		0.0	0.9		0.1	1.0		0.1	−1.0		0.1	0.6										
Case 2																								
0.369	0.3	3.6		0.0	1.7		0.1	1.2		0.1	1.1		0.3	1.4		0.3	1.5		0.5	2.1		0.7	3.4	
0.500	0.1	2.1	2.11	0.1	1.1	1.71	0.1	0.7	1.34	0.1	0.7	1.20	0.1	0.9	4.15	0.1	0.9	4.46	0.2	1.4	23	0.4	2.2	44
0.675	0.0	1.5		0.0	0.9		0.0	0.7		0.1	0.6		0.1	0.7		0.1	0.8		0.1	1.2		0.1	1.9	
0.776	0.0	1.4		0.0	0.9		0.0	0.7		0.0	0.6		0.1	0.8		0.1	0.8		0.1	1.2		0.1	1.9	
0.862	0.1	1.4		0.1	0.9		0.1	0.7		0.1	0.6		0.1	0.8		0.1	0.8		0.1	1.2		0.1	1.9	
1.048	0.0	1.5		0.0	1.0		0.0	0.8		0.1	0.7		0.1	0.9		0.1	0.9		0.1	1.3		0.1	2.1	
Case 3																								
0.369	0.2	3.4		0.1	1.7		0.0	1.0		0.1	0.7		0.2	0.8		0.4	1.4							
0.500	0.0	1.9	2.18	0.1	1.0	1.70	0.1	0.6	1.22	0.1	0.5	1.07	0.1	0.6	2.60	0.1	0.9	4.42						
0.675	0.0	1.4		0.1	0.8		0.0	0.6		0.1	0.5		0.1	0.5		0.1	0.8							
0.776	0.0	1.3		0.0	0.8		0.0	0.6		0.0	0.5		0.0	0.5		0.1	0.8							
0.862	0.1	1.4		0.1	0.9		0.1	0.6		0.1	0.5		0.1	0.6		0.1	0.9							
1.048	0.0	1.5		0.0	0.9		0.0	0.7		0.0	0.6		0.1	0.7		0.1	1.0							
Case 4																								
0.369	0.0	3.2		0.1	1.7		0.1	1.0		0.1	1.0		0.2	1.2										
0.500	0.1	1.8	2.05	0.1	1.0	1.73	0.1	0.7	1.77	0.1	0.7	1.48	0.1	0.8	3.84									
0.675	0.1	1.3		0.0	0.8		0.4	0.6		0.3	0.6		0.3	0.7										
0.776	0.0	1.3		0.0	0.8		0.0	0.6		0.0	0.6		0.1	0.7										
0.862	0.1	1.3		0.1	0.9		0.1	0.7		0.1	0.7		0.1	0.7										
1.048	0.0	1.4		0.0	0.9		0.0	0.7		0.0	0.7		0.0	0.8										

[a]Mode INDM = 2.

Table 3. Mean Relative Deviations (in Percent) between Simulated and Retrieved Data for Cases 1 (0.05–20 μm) and 5 (0.1–10 μm) and Different Selections of the Lower and Upper Radius Limits r_m, r_M[a]

	0.05–20			0.01–20			0.1–20			0.05–10			0.05–15			0.05–25			0.01–10			0.01–25		
λ (μm)	R	τ_A	v	R	τ_A	v	R	τ_A	v	R	τ_A	v	R	τ_A	v	R	τ_A	v	R	τ_A	v	R	τ_A	v
Case 1																								
0.369	0.0	1.7		0.1	5.0		0.1	−4.1		0.2	1.4		0.2	1.0		0.4	1.5		0.1	4.4		0.1	6.1	
0.500	0.0	1.0	1.67	0.1	3.4	1.50	0.1	−2.3	12.1	0.1	0.6	2.33	0.2	0.6	2.62	0.2	1.0	1.97	0.1	2.8	3.22	0.0	4.4	2.03
0.675	0.0	0.8		0.1	3.0		0.1	−1.6		0.1	0.2		0.1	0.6		0.0	1.0		0.0	2.2		0.1	4.0	
0.776	0.0	0.8		0.0	3.0		0.0	−1.5		0.1	0.0		0.0	0.6		0.0	1.1		0.1	2.0		0.1	3.9	
0.862	0.1	0.9		0.1	3.0		0.0	−1.4		0.0	0.0		0.1	0.7		0.1	1.1		0.1	1.9		0.1	4.0	
1.048	0.0	0.9		0.1	3.1		0.0	−1.4		0.1	−0.2		0.1	0.7		0.0	1.3		0.0	1.7		0.1	4.2	
	0.1–10			0.01–10			0.05–10			0.15–10			0.1–15			0.1–20			0.05–15			0.01–20		
	R	τ_A	v	R	τ_A	v	R	τ_A	v	R	τ_A	v	R	τ_A	v	R	τ_A	v	R	τ_A	v	R	τ_A	v
Case 5																								
0.369	0.1	0.2		1.1	3.9		0.4	2.0		0.4	−4.4		0.0	0.2		0.0	0.2		0.4	2.4		1.1	4.2	
0.500	0.1	−0.2	1.47	0.2	1.5	1.40	0.1	0.6	1.86	0.5	−1.1	35	0.1	−0.2	1.42	0.1	−0.1	1.36	0.1	0.7	2.42	0.2	1.5	2.14
0.675	0.0	−0.1		0.2	0.7		0.1	0.3		0.4	−0.1		0.0	0.0		0.0	0.0		0.1	0.4		0.2	0.8	
0.776	0.1	0.0		0.2	0.7		0.1	0.3		0.8	0.0		0.1	0.2		0.0	0.1		0.1	0.5		0.2	0.8	
0.862	0.2	0.0		0.1	0.5		0.2	0.2		1.0	−0.5		0.3	0.1		0.2	0.1		0.2	0.4		0.1	0.6	
1.048	0.1	0.0		0.1	0.4		0.1	0.2		0.6	−0.1		0.1	0.1		0.1	0.1		0.2	0.5		0.1	0.6	

[a]Mode INDM = 2.

Table 4. Sensitivity of the Retrieved Data to the Ground Albedo A for Cases 1 and 5 ($A = 0.25$)[a]

	0.200			0.213			0.225			0.237		
λ (μm)	R	τ_A	v	R	τ_A	v	R	τ_A	v	R	τ_A	v
Case 1												
0.369	0.1	8.0		0.2	6.6		0.4	5.4		0.2	3.0	
0.500	0.1	5.1	4.73	0.1	4.1	3.88	0.1	3.4	3.02	0.1	1.9	1.88
0.675	0.1	3.7		0.1	3.0		0.1	2.5		0.0	1.4	
0.776	0.1	3.3		0.1	2.7		0.1	2.3		0.0	1.4	
0.862	0.1	3.2		0.1	2.6		0.1	2.2		0.1	1.4	
1.048	0.1	3.0		0.1	2.5		0.1	2.1		0.0	1.4	
	0.250			0.263			0.275			0.287		
	R	τ_A	v	R	τ_A	v	R	τ_A	v	R	τ_A	v
0.369	0.0	1.7		0.1	0.3		0.1	−1.1		0.2	−2.4	
0.500	0.0	1.0	1.67	0.1	0.0	2.02	0.1	−0.8	2.63	0.1	−1.7	3.38
0.675	0.0	0.8		0.0	0.2		0.0	−0.5		0.1	−1.1	
0.776	0.0	0.8		0.0	0.2		0.1	−0.3		0.1	−0.8	
0.862	0.1	0.9		0.1	0.3		0.1	−0.2		0.1	−0.7	
1.048	0.0	0.9		0.1	0.5		0.1	0.0		0.1	−0.4	
	0.300			0.350								
	R	τ_A	v	R	τ_A	v						
0.369	0.2	−3.9		0.3	−10.2							
0.500	0.1	−2.7	4.28	0.2	−6.8	8.5						
0.675	0.1	−1.8		0.2	−4.6							
0.776	0.1	−1.4		0.2	−3.9							
0.862	0.1	−1.2		0.2	−3.5							
1.048	0.1	−0.9		0.2	−2.9							

	0.150			0.200			0.213			0.225		
λ (μm)	R	τ_A	v	R	τ_A	v	R	τ_A	v	R	τ_A	v
Case 5												
0.369	0.2	7.9		0.1	4.1		0.1	3.2		0.0	2.2	
0.500	0.3	4.3	15	0.2	2.1	8.36	0.1	1.5	6.46	0.1	1.0	4.74
0.675	0.2	2.7		0.1	1.3		0.1	1.0		0.1	0.6	
0.776	0.2	2.3		0.1	1.2		0.1	0.9		0.1	0.6	
0.862	0.1	2.0		0.1	1.0		0.1	0.8		0.1	0.5	
1.048	0.1	1.6		0.1	0.8		0.2	0.7		0.1	0.4	
	0.237			0.250			0.263			0.275		
	R	τ_A	v	R	τ_A	v	R	τ_A	v	R	τ_A	v
0.369	0.0	1.2		0.1	0.2		0.0	−0.7		0.1	−1.8	
0.500	0.1	0.4	3.03	0.1	−0.2	1.47	0.0	−0.8	1.57	0.1	−1.4	2.38
0.675	0.0	0.3		0.0	−0.1		0.0	−0.5		0.1	−0.8	
0.776	0.1	0.3		0.1	0.0		0.0	−0.3		0.1	−0.6	
0.862	0.1	0.3		0.2	0.0		0.1	−0.3		0.2	−0.6	
1.048	0.1	0.2		0.1	0.0		0.1	−0.2		0.1	−0.4	
	0.287			0.300			0.350					
	R	τ_A	v	R	τ_A	v	R	τ_A	v			
0.369	0.1	−2.7		0.1	−3.8		0.2	−7.8				
0.500	0.1	−1.9	2.86	0.1	−2.5	3.75	0.1	−4.9	6.87			
0.675	0.1	−1.2		0.1	−1.5		0.2	−2.9				
0.776	0.2	−0.8		0.1	−1.1		0.2	−2.2				
0.862	0.2	−0.8		0.1	−1.0		0.2	−2.0				
1.048	0.1	−0.5		0.1	−0.8		0.2	−1.5				

[a]Mode INDM = 2.

Table 5. Sensitivity to the Real Part m of the Complex Refractive Index for Cases 1 ($m = 1.48$) and 5 ($m = 1.50$)[a]

	1.33			1.38			1.43			1.48			1.53			1.58		
λ (μm)	R	τ_A	ν	R	τ_A	ν	R	τ_A	ν	R	τ_A	ν	R	τ_A	ν	R	τ_A	ν
Case 1																		
0.369	7.7	16		4.2	6.5		1.5	5.3		0.0	1.7		1.5	1.2		2.4	1.1	
0.500	7.3	8.3	50	4.7	2.4	30	2.1	2.0	15	0.0	1.0	1.67	1.3	2.2	20	2.4	3.8	35
0.675	6.7	5.1		4.1	1.0		1.6	0.9		0.0	0.8		1.1	2.5		1.8	4.6	
0.776	5.9	4.5		3.3	1.0		1.4	0.8		0.0	0.8		0.9	2.4		1.5	4.3	
0.862	5.5	4.3		2.9	1.0		1.3	0.8		0.1	0.9		0.7	2.4		1.2	4.2	
1.048	6.8	4.1		2.9	1.3		1.4	0.9		0.0	0.9		0.9	2.5		1.5	4.3	
	1.40			1.45			1.50			1.55			1.60					
	R	τ_A	ν	R	τ_A	ν	R	τ_A	ν	R	τ_A	ν	R	τ_A	ν			
Case 5																		
0.369	4.1	−2.3		1.5	−1.4		0.1	0.2		1.2	1.8		2.1	3.7				
0.500	4.7	−8.4	33	2.1	−4.3	15	0.1	−0.2	1.47	1.6	4.1	28	2.8	8.5	56			
0.675	4.5	−10.4		1.7	−5.2		0.0	−0.1		1.2	5.0		1.9	10.1				
0.776	3.8	−10.7		1.4	−5.2		0.1	0.0		0.9	5.2		1.4	10.1				
0.862	3.3	−11.0		1.2	−5.3		0.2	0.0		0.8	5.0		1.2	9.7				
1.048	3.6	−11.7		1.3	−5.7		0.1	0.0		0.8	5.4		1.2	10.3				

[a]Mode INDM = 2.

radius interval suitable for the treatment of a great variety of cases. Accordingly, we considered the effect of a different selection of r_m and r_M on the results of the inversion. Table 3 shows the results of cases 1 and 5 when the aerosol radius interval is changed. We show that results concerning τ_A and ν mainly deteriorate when r_m is greater than the true minimum radius, and $\epsilon(R)$ practically does not change; the best result for each case is obtained when the radius interval is slightly larger than the original one. The conclusion is that when turbid atmospheres are concerned, it can be reasonable to assume the two radius limits $r_m = 0.05$ and $r_M = 15$ μm.

To examine the consequences of a wrong evaluation of the ground albedo, we inverted the aureole data of cases 1 and 5 with a set of values of A that varied around the true values; results concerning only the mode INDM = 2 are given in Table 4. From these data one can see that when A departs from the true value ($A = 0.25$), the results of the inversion concerning τ_A and ν rapidly deteriorate, and $\epsilon(R)$ practically does not change; we also show that if we want to keep the relative deviations concerning τ_A within 5%, we have to determine A within 15%. By taking into account the required accuracy and the fact that the ground albedo that enters the aureole measurements has to be understood as an average over a few square kilometers of surface, we show that at present a suitable value of A can be obtained from the advanced very high resolution radiometer visible

Table 6. Sensitivity of the Retrieved Data to the Imaginary Park k of the Complex Refractive Index for Cases 1 ($k = 0.055$) and 5 ($k = 0.01$)[a]

	0.040			0.045			0.050			0.055			0.060			0.065		
λ (μm)	R	τ_A	ν	R	τ_A	ν	R	τ_A	ν	R	τ_A	ν	R	τ_A	ν	R	τ_A	ν
Case 1																		
0.369	0.5	−6.5		0.4	−3.5		0.2	−0.9		0.0	1.7		0.1	4.7		0.2	7.9	
0.500	0.2	−6.6	6.51	0.2	−3.9	4.52	0.1	−1.5	2.85	0.0	1.0	1.67	0.2	3.7	2.36	0.3	6.5	4.04
0.675	0.2	−6.8		0.1	−4.2		0.1	−1.7		0.0	0.8		0.1	3.5		0.2	6.3	
0.776	0.2	−7.0		0.1	−4.3		0.1	−1.8		0.0	0.8		0.1	3.6		0.1	6.5	
0.862	0.2	−7.1		0.1	−4.4		0.1	−1.8		0.1	0.9		0.1	3.7		0.1	6.6	
1.048	0.3	−7.3		0.2	−4.5		0.1	−1.8		0.0	0.9		0.1	3.9		0.1	7.0	
	0.0025			0.005			0.010			0.015			0.020					
	R	τ_A	ν	R	τ_A	ν	R	τ_A	ν	R	τ_A	ν	R	τ_A	ν			
Case 5																		
0.369	0.3	−5.7		0.2	−3.6		0.1	0.2		0.2	3.7		0.3	7.0				
0.500	0.2	−5.2	6.21	0.1	−3.4	4.23	0.1	−0.2	1.47	0.2	2.8	5.73	0.4	5.7	10.51			
0.675	0.2	−5.1		0.1	−3.3		0.0	−0.1		0.1	2.9		0.2	5.9				
0.776	0.2	−5.1		0.1	−3.3		0.1	0.0		0.1	3.2		0.2	6.3				
0.862	0.2	−5.3		0.2	−3.5		0.2	0.0		0.1	3.3		0.1	6.6				
1.048	0.2	−5.6		0.1	−3.7		0.1	0.0		0.1	3.6		0.2	7.1				

[a]Mode INDM = 2.

channels,[25] as in this way A can be reliably determined to within 10–15%.

To examine the consequences of a wrong evaluation of $\tilde{m}$ as input parameter, we inverted the aureole data of case 1 ($\tilde{m} = 1.48 - 0.055i$) and case 5 ($\tilde{m} = 1.5 - 0.01i$) with a set of values of m and k varying around the true values. Results concerning only the mode INDM = 2 are given in Tables 5 and 6 for m and k, respectively. From the data in Table 5 one can see that when m departs from the true value, the results of the inversion concerning τ_A and v, as well as those concerning R, rapidly deteriorate; if we want to keep the relative deviations concerning τ_A within 5%, we have to determine m within 3.5%. From the data in Table 6, one can see that when k departs from the true value, τ_A and v rapidly deteriorate, and R shows a very weak dependence; if we want to keep $\epsilon(\tau_A)$ within 5%, we have to determine k within 13% for case 1 ($k = 0.055$), and within 50% for case 5 ($k = 0.01$). By taking into account that m and k can usually be obtained from optical methods or chemical analysis[26–28] within 4% and 60%, respectively, we can conclude that a measure of these parameters has to be carried out together with aureole measurements.

We note that King and Herman[29] developed a statistical technique for inferring values of ground albedo and imaginary index of refraction of atmospheric aerosol particles from ground measurements of the ratio Φ between the hemispheric diffuse to directly transmitted solar flux densities; the ground albedo inferred from the ratio Φ represents a weighted average of the albedo over the entire area that affects the transfer of radiation.

A more interesting and completely different approach is to derive the above parameters from the aureole data themselves, by the use of the $R(\Theta)$ data in their entire possible angular range rather than on a restricted interval of Θ values ($3° \leq \Theta \leq 30°$) as done in this paper (for instance, when $\theta_0 = 60°$, $\Theta_{max} = 120°$, in the almucantar geometry); besides, measurements in the principal plane can help extend the value of Θ_{max}. Then, by taking into account that $R(\Theta)$ depends differently on the various parameters within different Θ intervals [at very small Θ, $R(\Theta)$ mainly depends on the size distribution, at small Θ it depends on $v(r)$ and m, at intermediate values of Θ it depends on A, and at the greatest scattering angles it depends on k], one can divide the $R(\Theta)$ data into three or four sets and search within each data set for the proper parameter. Of course, in each proper Θ interval for a given parameter there will be also the influence of the other parameters, but, if this last dependence is weak, it is possible that indicative or typical values of the relevant parameters could be sufficient; otherwise, more than one parameter should be retrieved from more than one Θ interval, simultaneously or through some iteration. This problem was considered in Nakajima *et al.*,[9] where the possibility of simultaneous estimation of the volume spectrum and the complex refractive index of aerosols was discussed with simulated data of aureole relative intensity and extinction; in Tanaka *et al.*[24] it was discussed further. If we examine our results in connection with this possible procedure, we show that, in the $3° \leq \Theta \leq 30°$ interval and within the assumptions concerning the INDM = 2 mode, the $R(\Theta)$ data do not depend on A (Table 4). They depend very slightly on k (Table 6) and substantially on m (Table 5).

In this section we considered only the mode INDM = 2, as through this mode an improved calibration of direct radiation can be carried out. More specifically, using the data on direct radiation from Eq. (1) requires setting up a procedure for reliably determining F_0 first and then extracting τ. The usual procedure for finding F_0 uses the Langley plot, which is based only on measurements of direct radiation, and which, for each wavelength, locates F_0 on an F–m graph for $m \rightarrow 0$, under the hypothesis $\tau = \text{const.}$; measurements last several hours, during which the last condition is almost never fulfilled, so that F_0 is usually determined to within at least 10%. The values of F_0 can be better determined with an improved method set up by Tanaka *et al.*,[30] which correctly extrapolates along an F–$m\tau$ graph, with τ derived from Eq. (3) as the ratio $[R(20°) - r(20°)]/\omega P(20°)$, where $R(20°)$ is measured, $r(20°)$ is computed with an aerosol model typical of the site and season, and $P_A(20°)$ is assumed to be independent of the size distribution and equal to 0.4; this procedure was shown to determine F_0 to within 1%. We propose an extension of the above approach, entirely based on measured data, that should function in the following way. A retrieval with only aureole data (INDM = 2) is first performed every 15 min, and the set of τ_A that is obtained is used to derive $m\tau$ and then F_0 by extrapolation along an F–$m\tau$ graph. Preliminary results based on experimental data showed this procedure to be very reliable. With the values of F_0 at hand, we determine through Eq. (1) a better set of τ_A values, which we again enter into the retrieval program but with INDM = 0 (both τ and R data) and then obtain the final results. In this situation the results will sharply improve, because τ_A is obtained from measurements and not retrieved, and the added extinction data enlarge the information content toward the side of small radii; the size interval becomes $0.01 \leq r \leq 10$ μm for Model 1 and $0.04 \leq r \leq 10$ μm for Model 2.

5. Conclusions and Remarks

The simulations carried out and shown in Section 3 for all four available modes demonstrate, within the limits of the cases considered, that the program set up for the inversion of the aureole data is accurate and efficient and is able to function reliably in several different situations. The selection of the input parameters, examined in Section 4 for the INDM = 2 mode only, showed that inaccurate values can cause great errors in the results, so that they have to be measured independently. A possible alternative ap-

proach, in which the whole information content of the aureole data is exploited, was anticipated. Finally, we proposed an improved procedure for calibrating the direct reading, which uses the optical thicknesses obtained from diffuse radiation through the mode INDM = 2.

We noted that besides the calibration for direct reading, there is a second calibration that concerns the determination of $\Delta\Omega$, which is entered into Eq. (3). A method recently set up by Nakajima consists of deriving $\Delta\Omega$ from the behavior of the solar intensity around the center of the solar disk. Both calibrations are at present being investigated with experimental data.

In this paper we elaborated data at the six wavelengths selected for the model of aureolometer used in our research. On the other hand, in Fig. 1 we show that both the $R(\Theta)$ curves and the τ_A values are not equally spaced and that around some wavelengths they are very close to each other; as the behavior and the closeness of both the $R(\Theta)$ curves and the τ_A values has to do with the information content of the optical data, and ultimately with the reliability of the retrieved results, we can reasonably deem that some wavelengths are redundant, and possibly that the number of wavelengths used can be reduced when the same information content and the same accuracy of the results are retained. In this way the aureolemeters, as well as the connected measurements and data elaboration, would be simplified. To investigate this point, we carried out inversions concerning the above-considered cases with the modes INDM = 2 and INDM = 0, by the use of several groups of wavelengths. Results showed that by the use of aureole data at the wavelengths 0.369 and 1.048 μm the accuracies of the quantities R, τ_A, and v, reconstructed at all six previously considered wavelengths, are almost the same as those obtained with actual data from all six wavelengths, and with only the 0.369-μm wavelength the accuracy gets only slightly worse. As this point has important practical implications, we plan to devote a separate paper to showing the full results and details.

In future programs the AUR.pack code and the inversion procedure will be improved along the following lines:

(a) Absorption by atmospheric gases was not considered in the present AUR.pack code, because a simulation carried out with the LOWTRAN 7 code for a midlatitude standard atmosphere characterized by τ_A (0.5 μm) = 0.2 showed that the contributions of the optical thickness as a result of gases to the total optical thickness are 0.0, 2.8, 6.3, 0.2, 1.6, and 1.8% for the six wavelengths considered; the absorption is mainly due to absorption by ozone. On the other hand, in an antarctic atmosphere with a τ_A (0.5 μm) = 0.02, the above contributions, for the six wavelengths considered, become 0, 5.8, 19, 0.7, 2.5, and 8%, respectively, so that in this situation gas absorption could have some influence on the final results. To this end, we have to take into account that the quantity R is relatively insensitive to this effect, because ozone absorption occurs above 20 km, whereas the majority of scattering by molecules and particles is confined to heights well below 20 km, so that O_3 mainly serves to attenuate the direct solar beam before the radiation interacts with the scattering atmosphere; as a consequence, it is expected that O_3 absorption will affect the diffuse and the direct flux densities by nearly the same fraction such that the diffuse–direct ratio will be largely insensitive to absorption by O_3. In conclusion, the effect of atmospheric gas absorption will only be introduced into the new version of the code when τ in Eq. (1) is corrected.

(b) Simulations will be used to study how to derive A and $\tilde{m}$ by increasing the interval of scattering angles at which R is measured and by locating the subintervals within which R has the maximum dependence on each parameter.

(c) The stability of the retrieval procedure will be improved when some constraint is imposed on the size distribution, such as positiveness or behavior at the boundaries.

(d) Polarization effects will be included.

Finally, let us recall that the aureole measurement performs an average over the whole layer of atmosphere, and this latter comes out to be highly dishomogeneous along the vertical, so one has to think of possibly connecting this study with more general research.

Appendix A: Geometry of Aureole Measurement

One method consists of carrying out measurements of intensity in the solar almucantar, that is, pointing from the origin along a conical surface with the same zenith angle θ_0 of the Sun (Fig. 4) and letting the azimuthal angle ϕ vary; another geometric situation in common use is making measurements in the

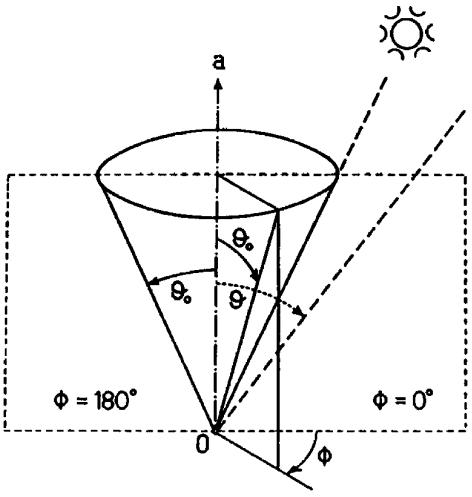

Fig. 4. Geometry concerning the measurement of the intensity in the solar almucantar and in the principal plane. The zenith axis is denoted by a, and the observer is at the origin O.

principal plane, that is, pointing along a plane with the same azimuth angle of the Sun and letting the zenith angle θ vary. When the aureolemeter points toward the Sun, it measures the direct radiation.

The scattering angle of the aerosol Θ is connected to θ_0, and to the observation angles θ and ϕ, by

$$\cos \Theta = \cos \theta_0 \cos \theta + \sin \theta_0 \sin \theta \cos \phi. \quad \text{(A1)}$$

In the almucantar geometry $(\theta = \theta_0)$ we have

$$\cos \Theta = \cos^2 \theta_0 + \sin^2 \theta_0 \cos \phi; \quad \text{(A2)}$$

from Eq. (A2), it turns out that $0° \le \Theta \le 2\theta_0$.

The function $\Theta(\phi)$ in Eq. (A2) is monotonically increasing for $0° \le \phi \le 180°$ and symmetric about $\phi = 180°$, so in this range we get $0° \le \Theta \le \Theta_{max} = 2\theta_0$; if we should assume for experimental or computational reasons that $0° < \phi < 180°$, we should compute Θ_{min} and Θ_{max} with Eq. (A2) as $\Theta_{min} = \Theta(\phi_{min})$, $\Theta_{max} = \Theta(\phi_{max})$. Figure 5 shows the behavior of the function $\Theta(\phi)$ for $\theta_0 = 30°$.

In the principal-plane geometry $\cos \Theta = \cos(\theta \mp \theta_0)$, the sign depending on whether $\phi = 0°$ or $\phi = 180°$, so that we have

$$\phi = 0°, \quad \theta_0 \le \theta \le 90° \rightarrow \Theta = \theta - \theta_0,$$
$$0° \le \Theta \le 90° - \theta_0, \quad \text{(A3)}$$

$$\phi = 0°, \quad 0° \le \theta \le \theta_0 \rightarrow \Theta = \theta_0 - \theta,$$
$$0° \le \Theta \le \theta_0, \quad \text{(A4)}$$

$$\phi = 180°, \quad 0° \le \theta \le 90° \rightarrow \Theta$$
$$= \theta_0 + \theta \rightarrow \theta_0 \le \Theta \le 90° + \theta_0; \quad \text{(A5)}$$

from Eqs. (A3)–(A5) it turns out that $0° \le \Theta \le \Theta_{max} = 90° + \theta_0$, so that the range of Θ values coming from the principal-plane geometry is always wider than that for the almucantar. Figure 6 shows the behavior of the function $\Theta(\theta)$ for $\theta_0 = 15°$.

The available solar zenith angles, and consequently the angles at which the aerosol scattering function can be recovered, depend on the latitude of the observation point L, the solar declination d, and the solar hour angle h (tables 169 and 170 of List[31]) and are given by $\cos \theta_0 = \sin L \sin d + \cos L \cos d \cos h$. In carrying out the measurements it is expedient to operate at zenith angles lower than $\theta_S \cong 70°$, to avoid the effects of the Earth's sphericity and refraction in the lower layers of the atmosphere; in this case $\theta_0 \le \theta_S$, from which $\Theta_{max} = \theta_S + \theta_0$ for the principal plane.

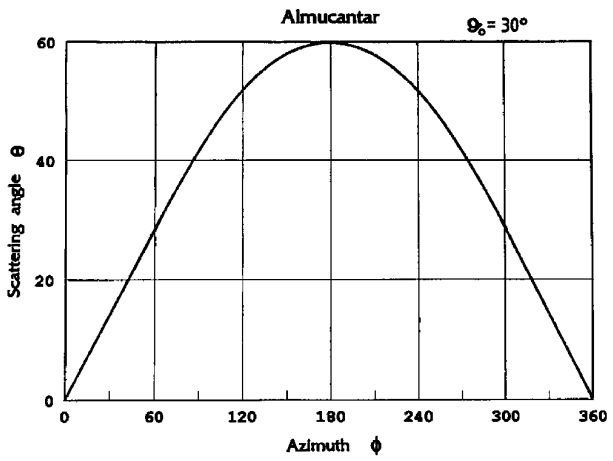

Fig. 5. Almucantar geometry: behavior of the scattering angle Θ with the azimuth angle ϕ, for $\theta_0 = 30°$.

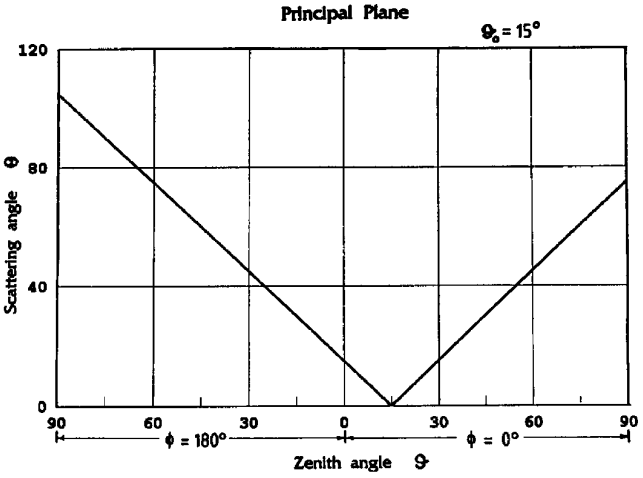

Fig. 6. Principal-plane geometry: behavior of the scattering angle Θ with the zenith angle θ, for $\theta_0 = 15°$.

This work was funded by the Commission of the European Communities under contract EV5V-CT93-0260 (Environment). We thank Enrico Lo Cascio for graphic work.

References

1. M. A. Box and A. Deepak, "Single and multiple scattering contributions to circumsolar radiation," Appl. Opt. **17,** 3794–3797 (1978).
2. K. Arao and M. Tanaka, "Dependence of the solar aureole upon the optical properties of aerosols and albedo of the ground surface," J. Meteorol. Soc. Jpn. **64,** 743–753 (1986).
3. K. Arao and M. Tanaka, "Photometric and colorimetric properties of the solar aureole," J. Meteorol. Soc. Jpn. **66,** 167–177 (1988).
4. A. Deepak, "Inversion of solar aureole measurements for determining aerosol characteristics," in *Inversion Methods in Atmospheric Remote Sounding,* A. Deepak, ed. (Academic, San Diego, Calif., 1977), p. 265.
5. M. A. Box and A. Deepak, "An approximation to multiple scattering in the Earth's atmosphere: almucantar radiance formulation," J. Atmos. Sci. **38,** 1037–1048 (1981).
6. D. Deirmendjian, "Use of scattering techniques in cloud microphysics research. 1. The aureole method," Rand Corp. Rep. R-590-PR (Rand Corp., Santa Monica, Calif., 1970).
7. J. A. Weinman, J. T. Twitty, S. R. Browning, and B. M. Herman, "Derivation of phase functions from multiply scattered sunlight transmitted through a hazy atmosphere," J. Atmos. Sci. **32,** 577–583 (1975).
8. J. T. Twitty, "The inversion of aureole measurements to derive aerosol size distributions," J. Atmos. Sci. **32,** 584–591 (1975).
9. T. Nakajima, M. Tanaka, and T. Yamauchi, "Retrieval of the optical properties of aerosols from aureole and extinction data," Appl. Opt. **22,** 2951–2959 (1983).

10. M. Tanaka and T. Nakajima, "Effects of oceanic turbidity and index of refraction of hydrosols on the flux of solar radiation in the atmosphere–ocean system," J. Quant. Spectrosc. Radiat. Transfer **18,** 92–111 (1977).
11. T. Nakajima and M. Tanaka, "Algorithms for radiative intensity calculations in moderately thick atmospheres using a truncation approximation," J. Quant. Spectrosc. Radiat. Transfer **40,** 51–69 (1988).
12. W. J. Wiscombe, "The delta-M method: rapid yet accurate radiative flux calculations for strongly asymmetric phase functions," J. Atmos. Sci. **34,** 1408–1422 (1977).
13. A. Deepak, M. A. Box, and G. P. Box, "Retrieval of aerosol size distributions from scattering and extinction measurements in the presence of multiple scattering," in *Remote Sensing of Atmospheres and Oceans,* A. Deepak, ed. (Academic, San Diego, Calif., 1980), p. 95.
14. G. E. Shaw, "Remote sensing of aerosol in the free atmosphere by passive optical techniques," in *Light Absorption by Aerosol Particles,* H. G. Gerber and E. E. Hindman, eds. (Spectrum, Hampton, Va., 1982), p. 335.
15. A. W. Peterson and E. L. Vande Noord, "Observations and analysis of the solar aureole in the near infrared," in *Atmospheric Aerosols: Their Formation, Optical Properties, and Effects,* A. Deepak, ed. (Spectrum, Hampton, Va., 1982), p. 287.
16. T. Nakajima, T. Takamura, M. Yamano, M. Shiobara, T. Yamauchi, R. Goto, and K. Murai, "Consistency of aerosol size distributions inferred from measurements of solar radiation and aerosols," J. Meteorol. Soc. Jpn. **64,** 765–776 (1986).
17. D. Tanré, C. Devaux, M. Herman, and R. Santer, "Radiative properties of desert aerosols by optical ground-based measurements at solar wavelengths," J. Geophys. Res. **93,** 14223–14231 (1988).
18. M. Shiobara, T. Hayasaka, T. Nakajima, and M. Tanaka, "Aerosol monitoring using a scanning spectral radiometer in Sendai, Japan," J. Meteorol. Soc. Jpn. **69,** 57–70 (1991).
19. J. T. Twitty, R. J. Parent, J. A. Weinman, and E. W. Eloranta, "Aerosol size distributions: remote determination from airborne measurements of the solar aureole," Appl. Opt. **15,** 980–989 (1976).
20. T. Nakajima, M. Tanaka, T. Hayasaka, Y. Miyake, Y. Nakanishi, and K. Sasamoto, "Airborne measurements of the optical stratification of aerosols in turbid atmospheres," Appl. Opt. **25,** 4374–4381 (1986).
21. M. Tanaka, T. Hayasada, and T. Nakajima, "Airborne measurements of optical properties of tropospheric aerosols over an urban area," J. Meteorol. Soc. Jpn. **68,** 335–344 (1990).
22. T. Hayasaka, T. Nakajima, and M. Tanaka, "The coarse particle aerosols in the free troposphere around Japan," J. Geophys. Res. **95,** 14039–14047 (1990).
23. E. P. Shettle and R. W. Fenn, "Models for the aerosols of the lower atmosphere and the effects of humidity variations on their optical properties," Rep. AFGL TR-79-0214 (U.S. Air Force Geophysics Laboratory, Hanscom Air Force Base, Mass., 1979).
24. M. Tanaka, T. Nakajima, and T. Takamura, "Simultaneous determination of complex refractive index and size distribution of airborne and water-suspended particles from light scattering measurements," J. Meteorol. Soc. Jpn. **60,** 1259–1272 (1982).
25. F. Cabot, G. Dedieu, and P. M. Maisongrande, "Surface albedo from space over Hapex Sahel sites," in *Proceedings of the 6th Advanced High Resolution Radiometer Data Users' Meeting* (EUMETSAT, Germany, 1993), p. 51.
26. G. Hänel, "Single scattering albedo, asymmetry parameter, apparent refractive index, and apparent soot content of dry atmospheric particles," Appl. Opt. **27,** 2287–2295 (1988).
27. H. Horvath, "Atmospheric light absorption—a review," Atmos. Environ. **27,** 293–317 (1993).
28. I. Sokolik, A. Andronova, and T. C. Johnson, "Complex refractive index of atmospheric dust aerosols," Atmos. Environ. **27,** 2495–2502 (1993).
29. M. D. King and B. M. Herman, "Determination of the ground albedo and the index of absorption of atmospheric particulates by remote sensing. Part 1: Theory," J. Atmos. Sci. **36,** 163–173 (1979).
30. M. Tanaka, T. Nakajima, and M. Shiobara, "Calibration of a Sunphotometer by simultaneous measurements of direct-solar and circumsolar radiations," Appl. Opt. **25,** 1170–1176 (1986).
31. R. J. List, *Smithsonian Meteorological Tables* (Smithsonian, Washington, D.C., 1958).